SPARSE RECONSTRUCTION-BASED ANGLE-RANGE-POLARIZATION-DEPENDENT BEAMFORMING WITH POLARIZATION SENSITIVE FREQUENCY DIVERSE ARRAY

Hui Chen *Huaizong Shao* *Wenqin Wang*

School of Communication and Information Engineering,
University of Electronic Science and Technology of China,
Chengdu, Sichuan, 611731, P.R. China

ABSTRACT

Traditional interference suppression approaches will enjoy the additional benefits when angle as well as polarization domain information are involved by polarization sensitive array (PSA). However, the information from range domain and its collaboration with other domains are rarely explored. In this paper, we present the polarization sensitive frequency diverse array (PSFDA) which combines frequency diverse array (FDA) and PSA for robust angle-range-polarization beamforming. To improve the angle-range-polarization resolution, the sparse reconstruction respective of compressive sensing is further applied. Theoretical analysis and simulation results demonstrate that our proposed algorithm can provide the good range-polarization resolution not just the target direction.

***Index Terms*—** Frequency diverse array (FDA), Polarization sensitive FDA (PSFDA), angle-range-polarization beamforming, sparse constraint, convex optimization, array pattern synthesis.

I. INTRODUCTION

To fully exploit the inherent information to improve the performance of an array, polarization signal processing technique [1], [2] has been explored to suppress interferences. Multi-domain signal processing [3], [4] can improve array performance by exploiting the multi-domain information such as spatial, time, polarization, frequency, etc. However, the advantages of range domain information has not been sufficiently explored.

Recently, a new array named frequency diverse array (FDA) which applies a small frequency increment, compared with the carrier frequency, between contiguous elements, has received much attention [5]–[7]. Two issued patents [6], [7] discussed the increased degrees of freedom (DOFs), and Mustafa *et al.* [8] analyzed the range, angle and time periodicity of FDA radiation pattern. Different from phased-array providing only angle-dependent beampattern, FDA provides angle-range-dependent beampattern [9]–[14].The angle-range-dependent beampattern makes the FDA have wide applications in target imaging [15], localization [16], [17], bistatic radar [12], [18]–[20], range-dependent interference suppression and target localization [16], [17]. However, existing literature concentrate on conceptual FDA system design, and little work about the joint applications of FDA and MIMO radars can be found [12]. Although the angle-range coupling in FDA will induce a degradation for the filter performance, it still better than a conventional uniform-linear phased-array. In this work, to further enhance the interference mitigation capability, we propose a polarization sensitive FDA (PSFDA) using polarization sensitive array (PSA). Furthermore, we propose an angle-range-polarization beamforming algorithm by jointly using the sparse reconstruction theory [21], [22] and convex optimization [23], the proposed angle-range-polarization-dependent beamforming can provide effectively suppress both clutter and interferences that is not accessible for conventional phased-array systems.

The remainder of this paper is organized as follows. Section II introduces the PSFDA array and formulates its received signal model. The resultant angle-range-polarization beamforming problem is analyzed in Section III, along with the proposed angle-range-polarization-dependent beamforming algorithm based on the sparse reconstruction. Extensive simulation results and discussions are provided in Section IV. Finally, conclusions are drawn in Section V.

II. PSFDA ARRAY AND SIGNAL MODEL

II-A. Frequency Diverse Array

Consider an M-element linear transmit FDA with uniform spacing $d = \lambda/2$ with λ being the wavelength. The radiated frequency of the m-th element is [5]

$$f_m = f_0 + (m-1)\cdot\Delta f,\ m = 1, 2, \ldots, M \tag{1}$$

where f_0 and Δf represent the carrier frequency and frequency increment, respectively. Taking the first element as the reference for the array, the phase difference between the m-th element and reference element for a given far-field point with direction θ and range r can be expressed as

$$\begin{aligned}\Delta\psi_{m-1} &= \psi_m - \psi_1\\ &\approx -\frac{2\pi f_0(m-1)d\sin\theta}{c} + \frac{2\pi r(m-1)\Delta f}{c}\\ &\quad -\frac{2\pi(m-1)^2\Delta f d\sin\theta}{c}\end{aligned} \tag{2}$$

using the approximation $r_m \approx r-(m-1)d\sin\theta$, where c is the speed of light. In (2), the first term is the same to conventional array factor seen frequently in phased-array. The second term shows that the FDA radiation pattern depends on both the range and the frequency increment. The third term is generally ignored due to a small frequency increment and far field assumption, such that $f_0 \gg \Delta f$ and source distance $r \gg dsin\theta$. Then the steering vector of a standard FDA can be expressed as (3).

$$\mathbf{a}(\theta, r) = \begin{bmatrix} 1 & e^{-j\upsilon_2} & \cdots & e^{-j\upsilon_M} \end{bmatrix}^T \tag{3}$$

where $\upsilon_m = \frac{2\pi f_0(m-1)d\sin\theta}{c} - \frac{2\pi r(m-1)\Delta f}{c}, m = 1, 2, ..., M$.

II-B. Polarization Sensitive Array

In a right-hand spherical coordinate system, with $\mathbf{u}$ representing the direction of propagation and the orthogonal basis defined by a pair of orthogonal component $\mathbf{v}_1$ and $\mathbf{v}_2$. The measurement model of the vector sensor is given by [24]

$$\begin{bmatrix} \mathbf{y}_E(t) \\ \mathbf{y}_H(t) \end{bmatrix} = \begin{bmatrix} \mathbf{I}_3 \\ (\mathbf{u}\times) \end{bmatrix} \mathbf{VQhs}(t) + \begin{bmatrix} \mathbf{e}_E(t) \\ \mathbf{e}_H(t) \end{bmatrix}, \tag{4}$$

where $\mathbf{I}_3$ is the third order identity matrix, and $(\mathbf{u}\times) = \begin{bmatrix} 0 & -u_z & u_y \\ u_z & 0 & -u_x \\ -u_y & u_x & 0 \end{bmatrix}$, u_x, u_y, u_z are the x, y, z components of the vector $\mathbf{u} = [\cos\theta\cos\phi, \sin\theta\cos\phi, \sin\phi]^T$, which indicates the unit direction vector from sensor to source, and the matrix $\mathbf{V}$, $\mathbf{Q}$ and vector $\mathbf{h}$ are given by

$$\mathbf{V} = \begin{bmatrix} \mathbf{V}_x^{(E)} \\ \mathbf{V}_y^{(E)} \\ \mathbf{V}_z^{(E)} \end{bmatrix} = \begin{bmatrix} -\sin\theta & -\cos\theta\sin\phi \\ \cos\theta & -\sin\theta\sin\phi \\ 0 & \cos\phi \end{bmatrix}, \tag{5}$$

$$\mathbf{Q} = \begin{bmatrix} \cos\alpha & \sin\alpha \\ -\sin\alpha & \cos\alpha \end{bmatrix}, \mathbf{h} = \begin{bmatrix} \cos\beta \\ j\sin\beta \end{bmatrix} \tag{6}$$

where $\theta \in [0, 2\pi), \phi \in [-\pi/2, \pi/2], \alpha \in (-\pi/2, \pi/2]$ and $\beta \in [-\pi/4, \pi/4]$ are the azimuth, elevation, polarized ellipse's orientation and eccentricity angles, respectively, $\mathbf{e}_E(t)$ and $\mathbf{e}_H(t)$ are the noise components of electric and magnetic fields, respectively.

Extending from (4) and assuming that the signal sources are narrowband, the measurement model of a vector sensor array in a multiple source environment, can be expressed as

$$\underbrace{\begin{bmatrix} \mathbf{y}_E(t) \\ \mathbf{y}_H(t) \end{bmatrix}}_{\mathbf{y}(t)} = \sum_{k=1}^{K} \mathbf{a}(\mathbf{\Lambda}_k)\mathbf{s}_k(t) + \underbrace{\begin{bmatrix} \mathbf{e}_E(t) \\ \mathbf{e}_H(t) \end{bmatrix}}_{\mathbf{n}(t)}, \tag{7}$$

$$\mathbf{a}(\mathbf{\Lambda}_k) = \mathbf{\Omega} \begin{bmatrix} \mathbf{I}_3 \\ (\mathbf{u}_k\times) \end{bmatrix} \mathbf{V}_k\mathbf{Q}_k\mathbf{h}_k$$

where $\mathbf{\Lambda}_k = [\theta_k, \phi_k, \alpha_k, \beta_k]$ denotes the direction and polarization parameters of the k-th source signal, $\mathbf{\Omega}$ is a $N \times 6$ selection matrix elements of "1" and "0", indicating the component of the electromagnetic field measured by the n-th sensor.

Extending the model to an array with M vector sensors, we can define the array response as

$$\mathbf{b}(\theta_k, \phi_k)\otimes\mathbf{a}(\theta_k, \phi_k), \tag{8}$$

where $\mathbf{a}(\theta_k, \phi_k) = \mathbf{\Omega} \begin{bmatrix} \mathbf{I}_3 \\ (\mathbf{u}_k\times) \end{bmatrix} \mathbf{V}_k$ embeds all the electromagnetic sources directional information, and the $\otimes$ is the *Kronecker Product*, and $\mathbf{b}(\theta_k, \phi_k) = \left[e^{j2\pi\mathbf{p}_1^T\mathbf{u}_k/\lambda}, e^{j2\pi\mathbf{p}_2^T\mathbf{u}_k/\lambda}, \ldots, e^{j2\pi\mathbf{p}_M^T\mathbf{u}_k/\lambda} \right]^T$ represents the phase of the planewave at the position $\mathbf{p}_i$ of the i-th vector sensor ($i = 1, \ldots, M$). Then the complex envelope of the measurements can be expressed as

$$\mathbf{y}(t) = \sum_{k=1}^{K} \left[\mathbf{b}(\theta_k, \phi_k)\otimes\mathbf{a}(\theta_k, \phi_k)\right] \mathbf{Q}_k\mathbf{h}_k\mathbf{s}_k(t) + \mathbf{n}(t). \tag{9}$$

According to the calculation rule of *Kronecker Product* $(A\otimes B)C = A\otimes(BC)$, where A is a column vector, (9) can be rewritten as

$$\begin{aligned} \mathbf{y}(t) &= \sum_{k=1}^{K} \mathbf{b}(\theta_k, \phi_k)\otimes\left[\mathbf{a}(\theta_k, \phi_k)\mathbf{Q}_k\mathbf{h}_k\right]\mathbf{s}_k(t) + \mathbf{n}(t) \\ &= \sum_{k=1}^{K} \mathbf{b}(\theta_k, \phi_k)\otimes\mathbf{g}(\theta_k, \phi_k, \alpha_k, \beta_k)\mathbf{s}_k(t) + \mathbf{n}(t). \end{aligned} \tag{10}$$

where $\mathbf{g}(\theta_k, \phi_k, \alpha_k, \beta_k) = \mathbf{a}(\theta_k, \phi_k)\mathbf{Q}_k\mathbf{h}_k$.

II-C. Signal Model of PSFDA

Assume an x-electric-component sensor and an y-electric-component sensor are used for each vector sensor, where each vector owns a different operating frequency, the PSFDA array arrangement with orthogonal dipole uniformly spaced is shown in Fig. 1. A joint angle-range-polarization steering vector of PSFDA is produced and thus the PSFDA transmitted signal is reformulated as

$$\begin{aligned} \mathbf{Z}(t) &= \sum_{k=1}^{K} \mathbf{c}(\mathbf{\Lambda}_k)\otimes\mathbf{b}(\theta_k, \phi_k)\mathbf{s}_k(t) + \mathbf{n}(t) \\ &= \sum_{k=1}^{K} \mathbf{c}(\mathbf{\Lambda}_k)\otimes\left[\mathbf{b}_{a,k}(\theta_k, \phi_k) \odot \mathbf{b}_{r,k}(\theta_k, \phi_k)\right]\mathbf{s}_k(t) + \mathbf{n}(t) \\ &= \sum_{k=1}^{K} \mathbf{g}(\vartheta_k)\mathbf{s}_k(t) + \mathbf{n}(t) \end{aligned} \tag{11}$$

where $\mathbf{c}(\mathbf{\Lambda}) = \begin{bmatrix} -\sin\theta & -\cos\theta\sin\phi \\ \cos\theta & -\sin\theta\sin\phi \end{bmatrix} \begin{bmatrix} \cos\alpha & \sin\alpha \\ -\sin\alpha & \cos\alpha \end{bmatrix} \begin{bmatrix} \cos\beta \\ j\sin\beta \end{bmatrix}$, $\mathbf{b}_{a,k}(\theta_k, \phi_k) = \begin{bmatrix} 1 & e^{-j\varphi_{a,k}} & \ldots & e^{-j(M-1)\varphi_{a,k}} \end{bmatrix}^T$ with $\varphi_{a,k} = 2\pi f_0 d\sin\theta_k\cos\phi_k/c$, $\mathbf{b}_{r,k}(\theta_k, \phi_k) = \begin{bmatrix} 1 & e^{j\psi_{r,k}} & \ldots & e^{j(M-1)\psi_{r,k}} \end{bmatrix}^T$ with $\psi_{r,k} = 2\pi r_k\Delta f/c$. In doing so, we get a spatio-polarized-range manifold $\mathbf{g}(\vartheta_k)$, which denotes the spatio-polarized-range information $\vartheta_k = (\theta_k, \phi_k, \alpha_k, \beta_k, r_k)$ for the k-th signal. The PSFDA steering vector depends on angle, range, frequency and polarization status as shown in (11). This means any parameter variations of the returned signals in these domain, will be reflected in PSFDA. These would serve as an effective discriminator in the mixed signals composed of target and inferences.

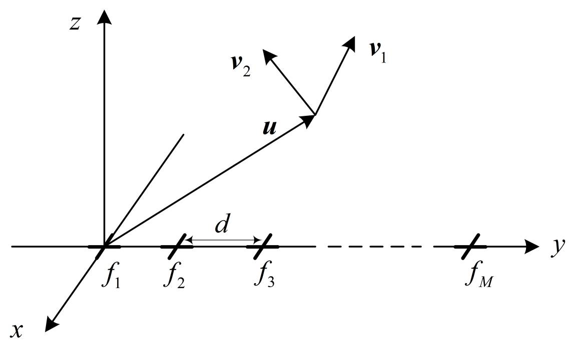

Fig. 1: Polarization Sensitive Frequency Diverse Array

III. PROPOSED ANGLE-RANGE-POLARIZATION BEAMFORMER

The PSFDA output of the M pairs of crossed dipoles, induced by the $K = J+1$ signals in the presence of additive noise $\mathbf{n}(t)$ is given by

$$\mathbf{Z}(t) = \mathbf{g}(\vartheta_s)\mathbf{s}(t) + \sum_{j=1}^{J} \mathbf{g}(\vartheta_j)\mathbf{i}_j(t) + \mathbf{n}(t),\ t = 1, \dots, T \tag{12}$$

where $\mathbf{g}(\vartheta_s)$ and $\mathbf{g}(\vartheta_j)$ $(j = 1, \dots, J)$ are the desired signal steering vector and interference steering vectors, respectively. The interest signal $\mathbf{s}(t)$, interferences $\mathbf{i}_j(t)$ $(j = 1, \dots, J)$ and $\mathbf{n}(t)$ are assumed to be zero-mean uncorrelated gaussian processes.

Let $\mathbf{R}_z$ denote the $2M \times 2M$ theoretical covariance matrix of the array snapshot vectors. We assume that $\mathbf{R}_z > 0$ is a positive definite matrix with the following form,

$$\mathbf{R}_z = \sigma_s^2 \mathbf{g}(\vartheta_s)\mathbf{g}^H(\vartheta_s) + \sum_{j=1}^{J} \sigma_j^2 \mathbf{g}(\vartheta_j)\mathbf{g}^H(\vartheta_j) + \mathbf{N} \tag{13}$$

where σ_s^2 and σ_j^2 $(j = 1, \dots, J)$ are the powers of the uncorrelated impinging signal and interferences, respectively, and $\mathbf{N}$ is the noise covariance matrix. Note that, $[\cdot]^T$ and $[\cdot]^H$ denote transpose and conjugate transpose respectively, lower and upper boldface letters are used for vectors and matrices, respectively, $\|\cdot\|_1$ and $\|\cdot\|_\infty$ indicate ℓ_1-norm and ℓ_∞-norm of a vector, respectively.

The sparse constraint encourages sparse distribution for all the array gains $\hat{\mathbf{G}} = [\mathbf{g}(\vartheta_1), \mathbf{g}(\vartheta_2), \dots, \mathbf{g}(\vartheta_L)]$ $(L \gg K)$, with fixed spacing. Actually, the array gains in the mainlobe are not sparse, that is, the element distribution of the beam pattern is dense as a solid block. So the ℓ_1-norm minimization based sparse constraint is added only on the array $\hat{\mathbf{G}}_s = [\mathbf{g}(\vartheta_1), \mathbf{g}(\vartheta_2), \dots, \mathbf{g}(\vartheta_{s-q}), \mathbf{g}(\vartheta_{s+q}), \dots, \mathbf{g}(\vartheta_L)]$ $(L \gg K)$ corresponding to sidelobe region of ϑ_s, where q is an integer corresponding to the bounds between the mainlobe and sidelobe of the beampattern. To further improve the beamforming performance, the ℓ_∞-norm minimization is also imposed on the sidelobe $\hat{\mathbf{G}}_s$. The sparse constraint beamformer based minimum variance angle-polarization-range sensitive (MVAPRS) can be recast,

$$\begin{aligned} \underset{\mathbf{w}}{\text{minimize}} \quad & \mathbf{w}^H \mathbf{R}_z \mathbf{w} + \xi \|\mathbf{w}^H \hat{\mathbf{G}}_s\|_1 \\ \text{subject to} \quad & \|\mathbf{w}^H \mathbf{g}(\varphi_s) - 1\|_\infty \le \eta \\ & \|\mathbf{w}^H \hat{\mathbf{G}}_s\|_\infty \le \eta \end{aligned} \tag{14}$$

where ξ is the weighting factor balancing the minimum variance constraint on total output energy and the sparse constraint on the beam pattern, the parameter η is selected according to desired array performance. The product $\mathbf{w}^H \hat{\mathbf{G}}_s$ indicates array gains of the sidelobe, and the sparse beam pattern constraint $\|\mathbf{w}^H \hat{\mathbf{G}}_s\|_1$ is imposed to further suppress the sidelobe level. As the new pattern shaping constraint in (14) fits the desired beam pattern better, the performance would be enhanced. This validity will be demonstrated by simulation examples in next section.

IV. SIMULATION RESULTS AND DISCUSSIONS

To evaluate the performance of the proposed beamforming technique, we carry out the statistical simulations in an ideal scenario without steering vector mismatch. In all numerical simulations, we consider an PSFDA with $M = 8$ pairs of crossed dipoles and spacing $d = 0.5m$ between adjacent dipole pairs. Suppose there is one desired signal and one undesired interference, and uncorrelated polarized signals which polarization ellipses are known. The signal-to-interference ratio (SIR) is fixed to -20dB. 100 independent simulation runs are performed with spatially white gaussian noise is also assumed.

We first consider a point source. The desired signal and interference have spatio-polarized characteristics $(\theta_s, \phi_s, \alpha_s, \beta_s, r_s) = (20°, 60°, -20°, 30°, 10km)$ and $(\theta_j, \phi_j, \alpha_j, \beta_j, r_j) = (20°, 60°, -20°, 30°, 8km)$, respectively. Fig.2(a) and (b) display the PSA beampattern and PSFDA beampattern, respectively. The S-shaped PSFDA beampattern provides angle-range-dependent beam, and hence it has additional degrees of freedom and potential applications in suppressing range interference and ambiguous clutter with the same angle but different range of the target, while the range-independent PSA beampattern has no such capabilities.

Besides, we compare the statical results for angle-range-dependent $block$-shaped beampattern obtained by the MVAPRS beamformer and our proposed beamformer by using the FDA with logarithmically increasing frequency offset. Fig. 3 displays the output SINRs versus SNR for $T = 100$. For a fixed SNR=0dB, the SINRs versus the number of snapshots T as shown in Fig. 4. The results clearly demonstrate that our proposed beamformer substantially outperforms the MVAPRS beamformer for SNR$>$ 0dB. In addition, since the proposed algorithm is convex optimization problem, which has been proved in [25], it can be efficiently resolved by CVX software [26].

V. CONCLUSIONS

In this paper, we first formulated PSFDA signal model, and then we proposed a corresponding beamformer based

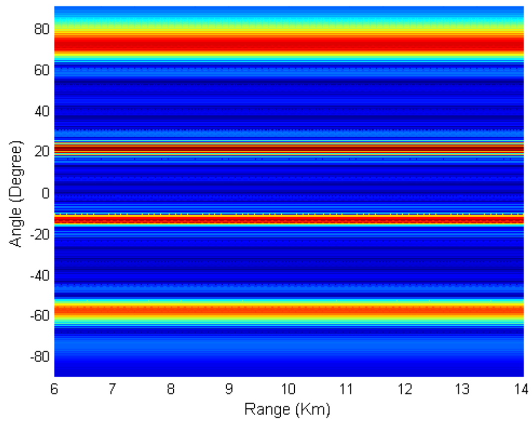

(a) PSA beampattern

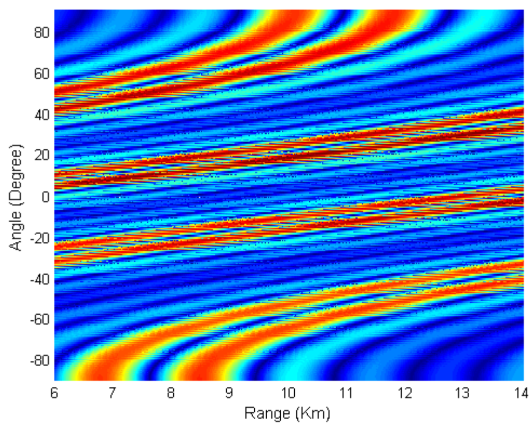

(b) PSFDA beampattern

Fig. 2: Comparative beampattern between PSA and PSFDA, where $\Delta f = 30kHz, N = 8, f_0 = 2GHz$, and $d = \lambda/2$.

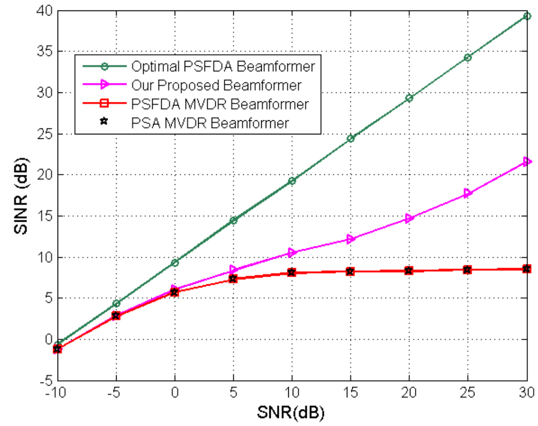

Fig. 3: SINR versus SNR (No-mismatch)

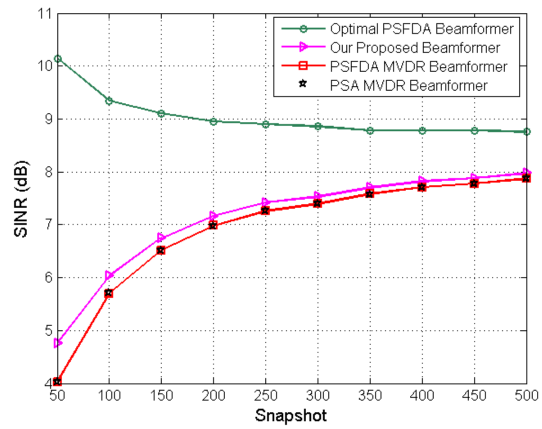

Fig. 4: SINR versus Number of Snapshots (No-mismatch)

on MVAPRS and sparse constraint. The proposed adaptive beamformer shows superiority to the conventional MVAPRS beamformer and PSA beamformer in terms of nulling interferences, while maintaining desired signal.

ACKNOWLEDGEMENT

This work was supported in part by the National Natural Science Foundation of China (61501089, 61471103), the Applied Basic Research Program of Sichuan Province (14JC0616), the Fundamental Research Fund for the Central Universities (ZYGX2014J008), and China Postdoctoral Science Foundation (2015M572462).

VI. REFERENCES

[1] X. P. Mao and Y. T. Liu, "Null phase-shift polarization filtering for high-frequency radar," *IEEE Transactions on Aerospace and Electronic Systems*, vol. 43, no. 4, pp. 1397 – 1408, 2007.

[2] X. P. Mao, A. J. Liu, H. J. Hou, H. Hong, R. Guo, and W. B. Deng, "Oblique projection polarisation filtering for interference suppression in high-frequency surface wave radar," *IET Radar Sonar Navigation*, vol. 6, no. 2, pp. 71 – 80, 2012.

[3] H. Hong, X. P. Mao, and C. Hu, "A multi-domain collaborative filter for hfswr based on oblique projection," in *2012 IEEE Radar Conference (RADAR)*, pp. 0907 – 0912, 2012.

[4] G. A. Fabrizio, G. J. Frazer, and M. Turley, "Stap for clutter and interference cancellation in a hf radar system," vol. 4, p. IV, 2006.

[5] P. Antonik, M. C. Wicks, H. D. Griffiths, and C. J. Baker, "Frequency diverse array radars," in *2006 IEEE Conference on Radar*, pp. 215–217, IEEE, 2006.

[6] M. C. Wicks and P. Antonik, "Frequency diverse array with independent modulation of frequency, amplitude,

and phase," U.S. Patent 7,319,427B2, January 15, 2008.

[7] M. C. Wicks and P. Antonik, "Method and apparatus for a frequency diverse array," U.S. Patent 7,511,665B2, March 31, 2009.

[8] S. Mustafa, D. Simsek, H. Altunkan, and E. Taylan, "Frequency diverse array antenna with periodic time modulated pattern in range and angle," in *2007 IEEE Conference on Radar*, pp. 427–430, IEEE, 2007.

[9] P. Antonik, M. C. Wicks, H. D. Griffiths, and C. J. Baker, "Range dependent beamforming using element level waveform diversity," in *Proceedings of the International Waveform Diversity and Design Conference*, pp. 1–4, 2006.

[10] W.-Q. Wang, "Range-angle dependent transmit beampattern synthesis for linear frequency diverse arrays," *IEEE Transactions on Antennas and Propagation*, vol. 61, no. 8, pp. 4073–4081, 2013.

[11] Y. Xu, X. Shi, J. Xu, and P. Li, "Range-angle-dependent beamforming of pulsed frequency diverse array," *IEEE Transactions on Antennas and Propagation*, vol. PP, no. 99, pp. 1–5, 2015.

[12] W. Q. Wang, "Phased-mimo radar with frequency diversity for range-dependent beamforming," *IEEE Sensors Journal*, vol. 13, no. 4, pp. 1320 – 1328, 2013.

[13] H. Shao, J. Li, H. Chen, and W.-Q. Wang, "Adaptive frequency offset selection in frequency diverse array radar," *IEEE Antennas and Wireless Propagation Letters*, vol. 13, no. 5, pp. 1405–1408, 2014.

[14] A. Basit, L. Qureshi, W. Khan, and S. khan, "Cognitive frequency offset calculation for frequency diverse array radar," in *12th International Bhurban Conference on Applied Sciences and Technology (IBCAST), 2015.*, pp. 641–645, IEEE, 2015.

[15] W.-Q. Wang, H. C. So, and H. Shao, "Nonuniform frequency diverse array for range-angle imaging of targets," *IEEE Sensors Journal*, vol. 14, no. 8, pp. 2469–2476, 2014.

[16] W. Q. Wang and H. Shao, "Range-angle localization of targets by a double-pulse frequency diverse array radar," *IEEE Journal of Selected Topics in Signal Processing*, vol. 8, no. 1, pp. 106–114, 2014.

[17] W. Q. Wang and H. C. So, "Transmit subaperturing for range and angle estimation in frequency diverse array radar," *IEEE Transactions on Signal Processing*, vol. 62, no. 8, pp. 2000 – 2011, 2014.

[18] P. F. Sammartino, C. J. Baker, and H. D. Griffiths, "Frequency diverse mimo techniques for radar," *IEEE Transactions on Aerospace and Electronic Systems*, vol. 49, no. 1, pp. 201–222, 2013.

[19] W. Khan, I. M. Qureshi, A. Basit, and M. Zubair, "A double pulse mimo frequency diverse array radar for improved range-angle localization of target," *Wireless Personal Communications*, vol. 82, no. 4, pp. 2199–2213, 2014.

[20] J. Xu, S. Zhu, and G. Liao, "Space-time-range adaptive processing for airborne radar systems," *IEEE Sensors Journal*, vol. 15, no. 3, pp. 1602–1610, 2015.

[21] D. L. Donoho, "Compressed sensing," *IEEE Transactions on Information Theory*, vol. 52, no. 4, pp. 1289–1306, 2006.

[22] S. Fortunati, R. Grasso, F. Gini, M. S. Greco, and K. Lepage, "Single-snapshot doa estimation by using compressed sensing," *Journal on Advances in Signal Processing*, vol. 2014, no. 16, pp. 1171–1173, 2014.

[23] S. Boyd and L. Vandenberghe, *Convex optimization*. Cambridge university press, 2004.

[24] A. Nehorai and E. Paldi, "Vector-sensor array processing for electromagnetic source localization," *IEEE Transactions on Signal Processing*, vol. 42, no. 2, pp. 376–398, 1994.

[25] H. Chen, Q. Wan, X. Zhang, and R. Fan, "Robust beamforming with inter-atom-interference mitigation approach for uniform circular arrays," *AEU-International Journal of Electronics and Communications*, vol. 69, no. 1, pp. 236–241, 2015.

[26] M. Grant, S. Boyd, and Y. Ye, "cvx users' guide for cvx version 1.1," *accessiable at: http://www. stanford. edu/~ boyd/index. html*, 2014.